Quench dynamics in a trapped Bose-Einstein condensate with spin-orbit coupling

Sheng Liu and Yongsheng Zhang*

Chinese Academy of Sciences Key Laboratory of Quantum Information, University of Science and Technology of China, Hefei 230026, China and Chinese Academy of Sciences Center for Excellence in Quantum Information and Quantum Physics, University of Science and Technology of China, Hefei 230026, China

(Received 30 November 2018; revised manuscript received 25 March 2019; published 13 May 2019)

We consider the phase transition dynamics of a trapped Bose-Einstein condensate subject to Raman-type spin-orbit coupling. By tuning the coupling strength the condensate is taken through a second-order phase transition into an immiscible phase. We observe the domain wall defects produced by a finite speed quench is described by the Kibble-Zurek mechanism, and quantify a power-law behavior for the scaling of domain number and formation time with the quench speed.

DOI: 10.1103/PhysRevA.99.053609

I. INTRODUCTION

Nonequilibrium physics is an active area of current research. While fewer tools exist for understanding out-of-equilibrium processes, universal behavior can still emerge. For instance, in the formation of topological defects in symmetry-breaking phase transitions, or in the self-similar growth of domains via defect annealing in phase-ordering dynamics.

The Kibble-Zurek mechanism (KZM) [1,2] is a theory used to describe the formation of defects at a phase transition in terms of the relevant critical exponents. There are many theoretical studies of the KZM in various systems, such as Landau-Zener transitions [3,4], temperature quenching across the Bose-Einstein condensation (BEC) transition [5], Ising model [6], and various types of spinor condensates [7–15]. To date experimental tests of the KZM have been performed in liquid crystals [16], cold atomic systems [17–19], linear optical systems [20], and ion Coulomb crystals [21]. A key challenge is to have a system in which there is good control over the rate at which the phase transition is crossed, and where the defects are relatively stable and able to be measured.

Experiments with cold atoms are able to dynamically engineer interesting single-particle properties and control interactions. This makes for a rich system to control and explore phase transition dynamics, particularly since topological defects can be readily detected in experiments [22–25].

In this paper we are motivated by the phenomenal development made in experiments producing spin-orbit coupling (SOC) terms in cold atom systems. We study the phase transition dynamics of a two-component BEC with a Raman-type SOC [26]. As the coupling strength is varied the system undergoes a quantum phase transition where the spin components change from being miscible to immiscible, also accompanied by changes in the momentum distribution. We study this problem in an experimentally realistic case of a quasi-(one-dimensional (1D) harmonic trap using the truncated Wigner method. We find that domain walls defects form separating the spin components in the immiscible phase. The number of these defects follows a scaling law related to the rate that the phase transition is crossed.

This article is organized as follows. In Sec. II, we briefly introduce some background on BEC with SOC and KZM, and we define the quench parameters. In Sec. III, we introduce the system parameters for numerical simulation, derive the Bogoliubov–de Gennes equations for SOC with BEC, introduced the truncated-Wigner method. In Sec. IV and V, we present and discuss the numerical analysis of our system.

II. BACKGROUND

A. Bose-Einstein condensate with SOC

The Raman-type SOC has been experimentally realized in cold atom systems [26]. Here a pair of lasers couple two internal atomic states denoted by 1 and 2 with Raman coupling strength Ω and two-photon momentum transfer of $\hbar k_r$. Here we focus on an elongated quasi-one-dimensional system in a harmonic trap of angular frequency ω_x and with the SOC momentum vector k_x taken to be along x.

Choosing $a_0 = \sqrt{\hbar/m\omega_x}$, $t_0 = 1/\omega_x$, and $E_0 = \hbar\omega_x$ as the units of length, time, and energy, respectively, the dimensionless time-dependent Gross-Pitaevskii equation (GPE) for this system is (e.g., see [26–29]) $i\partial_t\Psi = H\Psi$, where

$$H = \begin{pmatrix} \frac{k_x^2}{2} + \gamma k_x + I_1 & \frac{1}{2}\Omega \\ \frac{1}{2}\Omega & \frac{k_x^2}{2} - \gamma k_x + I_2 \end{pmatrix} + \frac{x^2}{2} + \frac{\delta}{2}\sigma_z, \quad (1)$$

$\Psi = (\psi_1, \psi_2)^T$, $I_j = g_{j1}|\psi_1|^2 + g_{j2}|\psi_2|^2$, with ψ_j being the condensate wave function for spin j and k_x denoting the quasimomentum, $\gamma = a_0 k_r$ is a dimensionless constant.

The interactions between the spin components are described by the short-ranged intra-species $\{g_{11}, g_{22}\}$ and the interspecies $g_{12} = g_{21}$ coupling constants. Here δ is the detuning of the Raman coupling, with σ_z the Pauli z matrix. From now on we set $\delta = 0$, and take the intraspecies interactions to be identical, i.e., $g_{11} = g_{22} = g$.

*yshzhang@ustc.edu.cn

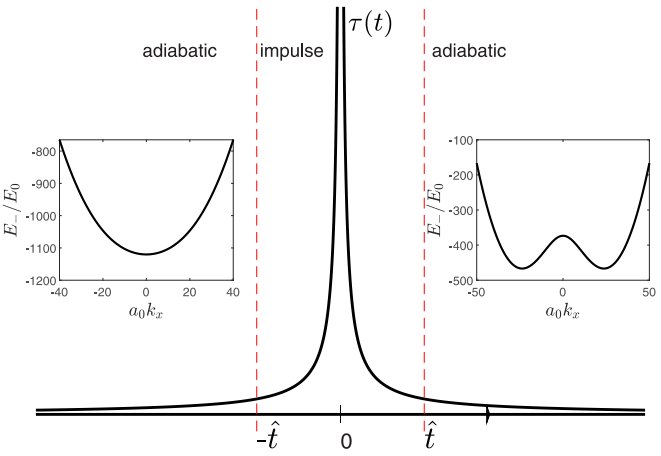

FIG. 1. Scheme of KZM. Inset: Lower branch E_- of the dispersion of the single-particle part of the SOC Hamiltonian in the absence of trapping for $\Omega = 1.5\Omega_c$ (left) and $\Omega = 0.75\Omega_c$ (right).

The dispersion relations for the single-particle part of the Hamiltonian (1) in the absence of the harmonic trap are

$$E_\pm = \frac{k_x^2}{2} \pm \sqrt{k_x^2\gamma^2 + \frac{\Omega^2}{4}}. \tag{2}$$

The lower branch E_- has one or two minima depending on the value of Ω. As shown in the insets of Fig. 1, for $\Omega > \Omega_c \equiv 2\gamma^2$, the minimum is at $k_x = 0$, and for $\Omega < \Omega_c$, the minima are at $k_x = \pm k_0$, where $k_0 = \sqrt{\gamma^2 - \frac{\Omega^2}{4\gamma^2}}$.

Including interaction effects this system exhibits three different phases that are accessible under appropriate conditions. Denoting the total density as $n = |\psi_1|^2 + |\psi_2|^2$, and defining $G_\pm = \frac{1}{4}n(g \pm g_{12})$, the system can access all three phases if the density is less than the critical value $n^c = \gamma^2 G_+/2gG_-$ as follows.

(i) *Stripe phase*: The condensate is in a superposition of $\pm k_0$ momentum states, occurring for $\Omega < \Omega_1^c$. In this state the overall magnetization of the state is zero, i.e., $M_z \equiv \int dx(|\psi_1|^2 - |\psi_2|^2) = 0$.

(ii) *Plane-Wave phase*: The condensate prefers to occupy either of the $\pm k_0$ momentum states when $\Omega_1^c < \Omega < \Omega_2^c$. This phase breaks the spin symmetry with the magnetization M_z being nonzero, taking the value $M_z = \pm k_0 N$, where $N = \int dx\, n$.

(iii) *Zero-Momentum phase*: When $\Omega > \Omega_2^c$, $k_0 = 0$ and the condensate occupies the zero-momentum mode. This state has $M_z = 0$, although exhibits transverse magnetization.

In describing the phases above we introduced $\Omega_1^c \equiv \sqrt{\frac{8G_-(\gamma^2+G_+)(\gamma^2-2G_-)}{G_++2G_-}}$ and $\Omega_2^c \equiv 2(\gamma^2 - 2G_-)$. We also note that the transition from zero-momentum phase to plane-wave phase is second order [29,30] and we can explore KZM in this scenario.

The system breaks a Z_2 symmetry and chooses between the two possible ground states when it crosses from zero-momentum phase to plane-wave phase. These ground states can be distinguished by their momenta and spin composition (magnetization). When phase transition is crossed at finite rate, the ground-state choice is made locally in the system, giving rise to domains. We characterize the local order using normalized magnetization density

$$j_z(x) = \frac{|\psi_1(x)|^2 - |\psi_2(x)|^2}{|\psi_1(x)|^2 + |\psi_2(x)|^2}, \tag{3}$$

which will gain a nonzero value of either $\pm k_0/\gamma$ in the plane-wave phase.

B. Kibble-Zurek mechanism

For a homogeneous system (without a trap) crossing a second-order phase transition point, we can introduce a parameter ϵ to quantify the distance from the critical point. For instance, ϵ could be some thermodynamic parameters like temperature (e.g., [31]) or some Hamiltonian control parameter (e.g., [18]). Near the critical point the correlation length and relaxation time diverge as

$$\xi = \xi_0/|\epsilon|^\nu, \quad \tau = \tau_0/|\epsilon|^{\nu z}, \tag{4}$$

respectively, where ξ_0 and τ_0 depend on the specific system, the critical exponents ν and z are determined by the universality class of the phase transition.

According to KZM, when the phase transition is crossed, critical slowing-down intervenes [31]: As the relaxation time diverges correlations freeze in at a length scale determined by the speed that the system crosses the transition. Thus different parts of the system make different choices for the symmetry broken order parameter and domains of order are produced.

The frozen time $\hat{t}$ is a pivotal quantity in KZM, defining when the evolution becomes nonadiabatic (see Fig. 1). We identify this time by equating the quench time scale $\epsilon/\dot{\epsilon}$ to the relaxation time

$$\tau(\hat{t}) = \epsilon(\hat{t})/\dot{\epsilon}(\hat{t}). \tag{5}$$

For a linear quench $\epsilon = t/\tau_q$, where τ_q is the quench time, we obtain $\hat{t} = (\tau_0\tau_q^{\nu z})^{\frac{1}{1+\nu z}} \sim \tau_q^{\frac{\nu z}{1+\nu z}}$, and the correlation length that freezes in at $\hat{t}$ is

$$\hat{\xi} = \xi_0(\tau_q/\tau_0)^{\frac{\nu}{1+\nu z}}, \tag{6}$$

then, for 1D system, the defects number is given by

$$N_q = L/\hat{\xi} \sim \tau_q^{-\frac{\nu}{1+\nu z}}, \tag{7}$$

where L is the system size.

Above we talked about KZM in a uniform system, but it is always a inhomogeneous system we need to test our results in experiments. For a trapped BEC system, the critical phase transition point is different everywhere, and so is the sound velocity, which is the key parameter in KZM. There are several papers that addressed the inhomogeneous effect in KZM [32–34], the results indicate that there will be a different scaling law for the inhomogeneous system which will give different scaling exponents ν and z. They found the system is well described by homogeneous KZM (HKZM) for fast quench times, and the inhomogeneous KZM (IKZM) will be needed for slow-enough quench times.

Let us consider the case where we include the trapping potential and the external quench parameter is homogeneous

(not depends on position) and linear in time

$$\Omega(t) = \frac{\Omega_f - \Omega_i}{\tau_q} t + \Omega_i, \tag{8}$$

the local critical point depends on the position

$$\Omega_c(x) = \Omega_c - 4G_-(x), \tag{9}$$

the change rate for the quench parameter is

$$v_0 = \frac{\Omega_i - \Omega_f}{\tau_q}, \tag{10}$$

this gives us the speed of the front where the critical Rabi coupling strength is reached

$$v_p(x) = \frac{v_0}{4G'_-(x)}. \tag{11}$$

The Thomas-Fermi approximation is valid for zero-momentum phase (Phase III) since in this phase the two components have the same density distribution, and the density profile is given like $n(x) = C(1 - x^2/R_{\rm TF}^2)$, where C is a normalization constant. Define $\Delta g = g_{12} - g$, then the speed of front follows:

$$v_p(x) = \frac{v_0 R_{\rm TF}^2}{2C\Delta g x} = \frac{(\Omega_i - \Omega_f)R_{\rm TF}^2}{2\tau_q C \Delta g x}, \tag{12}$$

we can see the speed of front in the trap center diverges, this means the defects form first at the trap center, and only form within the radius that satisfies condition that the speed of sound is smaller than that of the front. According to [33], for slower-enough quench rate, the scaling law between the quench time τ_q and number of defects N_q is

$$N_q \sim \tau_q^{-\frac{1+2\nu}{1+z\nu}}, \tag{13}$$

in the above formula, the number of defects is obtained within a region that the size of it depends on the quench rate.

C. Quench parameters

In our simulation, the quench parameter is defined as

$$\epsilon = \frac{\Omega - \Omega_c}{\Omega_c}, \tag{14}$$

where $\Omega_c = 2\gamma^2$ and Ω is linearly quenched from $\Omega_i = 1.5\Omega_2^c$ to $\Omega_f = 0.75\Omega_2^c$, so we have

$$\Omega(t) = \frac{\Omega_f - \Omega_i}{\tau_q} t + \Omega_i, \tag{15}$$

from above we can get the time t_C that $\Omega(t_C) = \Omega_c$

$$t_C = \frac{\Omega_c - \Omega_i}{\Omega_f - \Omega_i}\tau_q. \tag{16}$$

From Sec. II B, we know that the correlation length and relaxation time satisfy $\tau = \tau_0/|\epsilon|^{\nu z}$ and $\xi = \xi_0/|\epsilon|^{\nu}$. We choose $t = t_C + t'$, then

$$\epsilon(t) = \epsilon(t_C + t') \equiv \eta(t'), \tag{17}$$

this gives us

$$\tau = \tau_0/|\eta|^{\nu z}. \tag{18}$$

The frozen time is defined as $\tau(t') = \frac{\eta(\hat{t}')}{\dot{\eta}(\hat{t}')}$, we get

$$\hat{t}' = \left(\frac{\Omega_c}{\Omega_i - \Omega_f}\right)^{\nu z/1+\nu z} \tau_0^{\frac{1}{1+\nu z}} \tau_q^{\frac{\nu z}{1+\nu z}}. \tag{19}$$

Finally, we have

$$\hat{t} - t_C = \left(\frac{\Omega_c}{\Omega_i - \Omega_f}\right)^{\nu z/1+\nu z} \tau_0^{\frac{1}{1+\nu z}} \tau_q^{\frac{\nu z}{1+\nu z}} \propto \tau_q^{\frac{\nu z}{1+\nu z}}, \tag{20}$$

and

$$|\Omega(\hat{t}) - \Omega_c| = \Omega_c \left(\frac{\Omega_c}{\Omega_i - \Omega_f}\right)^{\frac{-1}{1+\nu z}} \tau_0^{\frac{1}{1+\nu z}} \tau_q^{-\frac{1}{1+\nu z}} \propto \tau_q^{-\frac{1}{1+\nu z}}. \tag{21}$$

III. QUENCH DYNAMICS OF TRAPPED BEC WITH SOC

A. System parameters

As described above, $G_- = n(x)(g - g_{12})/4$ depends on position if the system is trapped, so the critical $\Omega_2^c(x) = 2[\gamma^2 - 2G_-(x)]$ depends on position, where $n(x)$ is taken to be the initial total density. To implement a quench we ramp down Ω from an initial value $\Omega_i = 1.5\Omega_2^c(x)$ in the zero-momentum phase to $\Omega_f = 0.75\Omega_2^c(x)$ in the plane-wave phase. In the ramp Ω changes linearly in time over a time interval τ_q that we take to define the quench time, i.e., $\Omega(t) = \max([\Omega_f, \Omega_i - (\Omega_i - \Omega_f)t/\tau_q)])$, where $t \geqslant 0$. Here we study quench times ranging from 10 to 1000 ms.

We consider a system of $N = 10^4$ ^{87}Rb atoms with trap frequency $\omega_x = 2\pi \times 5$ Hz, $\omega_y = \omega_z = 2\pi \times 2$ kHz, and interspecies interaction strength of $g_{12} = 1.05g$, with $g = 4\pi a_s \hbar^2/m$, where $a = 100.86\, a_0$ and a_0 is the Bohr radius. We consider the SOC to be produced by two $\lambda = 784$ nm lasers crossed at an angle of $\pi/2$, so the recoil momentum is $k_r = \sqrt{2}\pi/\lambda$. Under this condition, $G_- = n(g - g_{12})/2 = ng_s/2$ (where $g_s = g - g_{12}$) is small and negative, this gives $\Omega_1^c < 0$, so we can exclude the stripe phase from our analysis.

To simulate the quench dynamics we use the truncated-Wigner method [35], whereby initial noise is added to the Bogoliubov quasiparticle modes to simulate the effects of vacuum fluctuations. The initial condensate (at $\Omega = 1.5\Omega_2^c$) is obtained by imaginary time propagation, and then the quasiparticle modes are calculated by numerical diagonalization and used to add noise to construct the initial field. The simulation is then performed by evolving the initial field in real time with the GPE as Ω is linearly ramped to effect the quench.

B. Bogoliubov–de Gennes equations for SOC BEC

In the following we use Bogoliubov–de Gennes (BdG) method [36] to get the excitation energies and the corresponding wave functions.

For the ground-state wave function Φ_g of SOC BEC, we have the stationary GPE

$$\mu\Phi_g = H\Phi_g, \tag{22}$$

where $\Phi_g = (\phi_{1g}, \phi_{2g})^T$. We assume the time-dependent wave function is

$$\Psi = [\Phi_g + \delta\Psi]\exp(-i\mu t), \tag{23}$$

where $\delta\Psi$ is the fluctuation.

Substitute the above wave function into the time-dependent Gross-Pitaevskii equation and make use of the stationary GPE, we get two equations on $\delta\Psi$

$$i\frac{\partial}{\partial t}\delta\psi_1 = L_1\delta\psi_1 + g\phi_{1g}^2\delta\psi_1^* + \left[g_{12}\phi_{1g}\phi_{2g}^* + \frac{\Omega}{2}\right]\delta\psi_2 + g_{12}\phi_{1g}\phi_{2g}\delta\psi_2^* \tag{24}$$

and

$$i\frac{\partial}{\partial t}\delta\psi_2 = L_2\delta\psi_2 + g\phi_{2g}^2\delta\psi_2^* + \left[g_{12}\phi_{1g}^*\phi_{2g} + \frac{\Omega}{2}\right]\delta\psi_1 + g_{12}\phi_{1g}\phi_{2g}\delta\psi_1^*, \tag{25}$$

where $L_1 = \frac{k_x^2}{2} + \gamma k_x + V_{\text{trap}} + g_{12}|\phi_{2g}|^2 + 2g|\phi_{1g}|^2 - \mu$ and $L_2 = \frac{k_x^2}{2} - \gamma k_x + V_{\text{trap}} + g_{12}|\phi_{1g}|^2 + 2g|\phi_{2g}|^2 - \mu$.

We choose the following excitation form [37]:

$$\begin{aligned}\delta\psi_1 &= u_1(x)\exp(-i\omega t) - v_1^*\exp(i\omega t),\\ \delta\psi_2 &= u_2(x)\exp(-i\omega t) - v_2^*\exp(i\omega t).\end{aligned} \tag{26}$$

Substitute Eq. (26) into Eqs. (24) and (25) and compare the coefficients, we get the BdG matrix equation for $[u_1(x), v_1(x), u_2(x), v_2(x)]^T$

$$M_{\text{BdG}}\begin{pmatrix}u_1\\ v_1\\ u_2\\ v_2\end{pmatrix} = \omega\begin{pmatrix}u_1\\ v_1\\ u_2\\ v_2\end{pmatrix}, \tag{27}$$

in which M_{BdG} is the BdG matrix

$$\begin{pmatrix}A+B & -D & F & -E\\ D^* & -A^*-B^* & E^* & -F^*\\ F^* & -E & A+C & -G\\ E^* & -F & G^* & -A^*-C^*\end{pmatrix}, \tag{28}$$

where $A = \frac{k_x^2}{2} + \gamma k_x$, $B = V_{\text{trap}} + 2g|\phi_{1g}|^2 + g_{12}|\phi_{2g}|^2 - \mu$, $C = V_{\text{trap}} + 2g|\phi_{2g}|^2 + g_{12}|\phi_{1g}|^2 - \mu$, $D = g\phi_{1g}^2$, $G = g\phi_{2g}^2$, $E = g_{12}\phi_{1g}\phi_{2g}$, $F = \frac{\Omega}{2} + g_{12}\phi_{1g}\phi_{2g}^*$.

Substitute the ground-state wave function $\{\phi_{1g}, \phi_{2g}\}$ into Eq. (27), then diagonalize the BdG matrix to get the collective excitation energies $\{\omega_j\}$ and the corresponding excitation wave functions $\{u_{1j}, v_{1j}, u_{2j}, v_{2j}\}$.

After we get the excitation energies and excitation wave functions, we form the initial wave function for the real time evolution as follows:

$$\begin{aligned}\psi_1(x) &= \psi_{1g} + \sum_{j=1}[\beta_j u_{1j}(x)e^{-i\omega t} - \beta_j^* v_{1j}^*(x)e^{i\omega t}],\\ \psi_2(x) &= \psi_{2g} + \sum_{j=1}[\alpha_j u_{2j}(x)e^{-i\omega t} - \alpha_j^* v_{2j}^*(x)e^{i\omega t}],\end{aligned} \tag{29}$$

the coefficients $\{\alpha_j, \beta_j\}$ are random numbers sampled from the Wigner distribution for zero-temperature thermal state [38], i.e.,

$$W(\alpha, \alpha^*) = \frac{2}{\pi}\exp(-2|\alpha|^2). \tag{30}$$

IV. NUMERICAL RESULTS

A. Scaling laws

For each quench time τ_q we conducted 100 trajectories of the truncated Wigner simulations which we use to compute statistics. In each trajectory a different sampling of noise is used to construct the initial condition, and has the effect of providing a different seed for the growth of the symmetry-breaking domains during the quench. In the upper panel of Fig. 2 we show single realization of $j_z(x)$ for several quench times. We can clearly see the typical domain sizes and the number of domains vary with time. The domains are less prominent towards the edge of the condensate because the density is lower there. Noise or thermal excitations from the quench can be more important in the low density wings making the identification of the domains difficult in this region, so we only count the domains number within the Thomas-Fermi radius. As described before, the single-particle dispersion transitions from having a single minimum at $k_0 = 0$ to having two degenerate minima at $k = \pm k_0$ in the quench process. According to KZM, there will be a delay for the momentum bifurcation for finite quench speed, and this delay effect can be seen in the lower panel of Fig. 2 and we can use this effect to determine the domain formation time as we will discuss below.

To extract the power law, we count the number of domains N_q by counting how many times $j_z(x)$ crosses zero within certain region. To make sure the growth of domains ceased to increase, we take N_q to be the mean zero-crossing number from time $t = \tau_q$ to $t = \tau_q + 20$ ms.

We can explore the phase-transition scaling by seeing how the number of domains produced in the quench depends on the quench time. The number of domains will scale as $N_q \sim 2R/\hat{\xi} \sim \tau_q^{-\nu/(1+\nu z)}$, where R is the region's radius and $\hat{\xi}$ is correlation length at frozen time $\hat{t}$ (6), which depends on the quench time. A power-law fit to the results summarized in Fig. 3 allows us to extract the exponent $\frac{\nu}{1+\nu z} = 0.25 \pm 0.05$ for $R = R_{\text{TF}}$. This means for sufficient quick quench the system is well described by HKZM [39]. As the quench time increases, the scaling exponent begins to deviate from the predication of HKZM, as seen in Fig. 3, the red-dashed line gives us a scaling exponent $\alpha = 0.42 \pm 0.04$. This reason is that the causality determines the effective size of the area where the defects form, leading to a more pronounced dependence on the quench time.

When the system crossed the phase transition point with finite speed, according to KZM, there will be two peaks in the momentum distribution, we calculated the time-dependent second moment of the momentum distribution $\sigma_k^2 = \int k^2 n(k)dk / \int n(k)dk - (\int kn(k)dk / \int n(k)dk)^2$, where $n(k) = |\phi_1(k)|^2 + |\phi_2(k)|^2$, and $\phi_j(k)$ are the Fourier transformations of wave functions $\psi_j(x)$. In the inset of Fig. 4, we can clearly see a sharp slope, and we choose a threshold 50 to indicate the domains formation time $\hat{t}$.

In Fig. 4 we plot $\hat{t} - t_C$ versus the quench time τ_q and we extract another exponent $\frac{\nu z}{1+\nu z} = 0.52 \pm 0.03$. From the above two scaling laws, we can extract the scaling exponents $\nu = 0.52$ and $z = 2.08$. These two scaling exponents fit the prediction of homogeneous KZM. In our simulation, we use position-dependent quench parameter Ω to reduce the effect

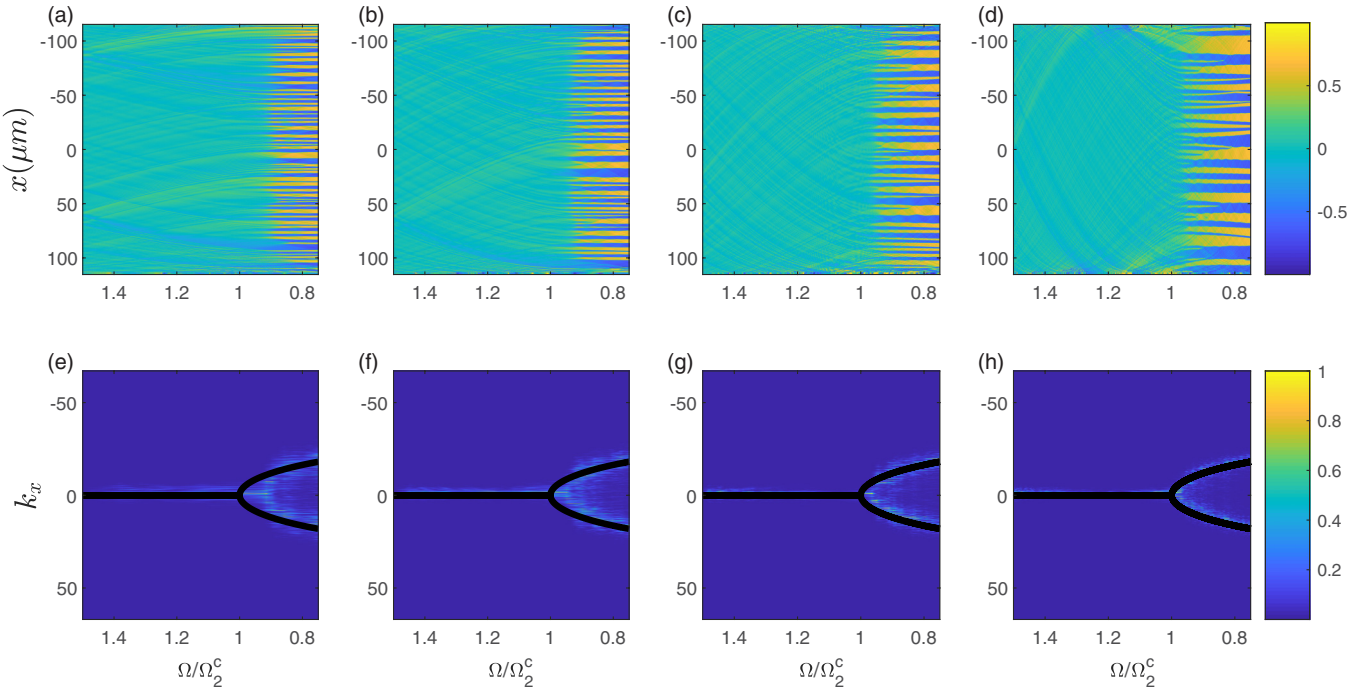

FIG. 2. Upper panel: Local magnetization $j_z(x)$ versus Ω/Ω_2^c for quench time (a) $\tau_q = 40$ ms, (b) $\tau_q = 80$ ms, (c) $\tau_q = 160$ ms, and (d) $\tau_q = 320$ ms. Lower panel: Bifurcation of momentum distribution versus Ω/Ω_2^c for quench time (e) $\tau_q = 40$ ms, (f) $\tau_q = 80$ ms, (g) $\tau_q = 160$ ms, and (h) $\tau_q = 320$ ms. The black solid curve indicate the instantaneous momentum distribution. We only plotted the region within the Thomas-Fermi radius.

caused by the trap. Our results show that it is impossible to get rid of this inhomogeneous effect totally, this inhomogeneous effect is more important for slow-enough quench times.

B. Inhomogeneity of the system

For quench time τ_q between ∼10 and ∼100 ms, our quench scheme shows that the system is well described by HKZM, as in [15,40]. But for quench time $\tau_q < 10$ ms, the domains number saturated to a constant value as we can see from the inset of Fig. 3, this constant value is reaching the maximum domains number allowed by the system. In this region, the KZM will not give the correct value due to the miscounting of domain number. When the quench time $\tau_q > 150$ ms,

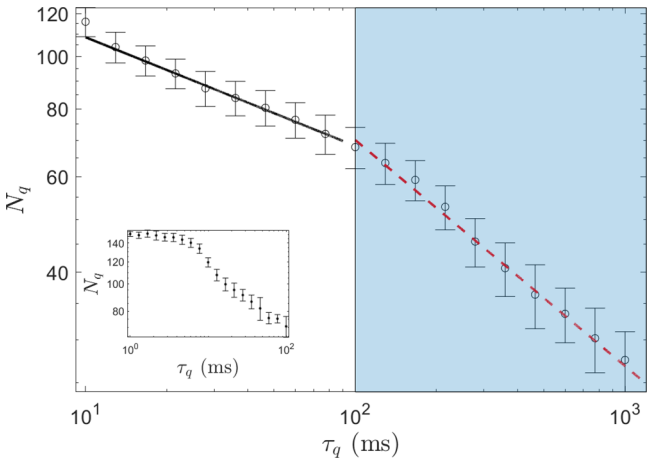

FIG. 3. Domains number N_q versus quench time τ_q. Circles with error bars correspond to numerical results. Black-solid line is the fitting for τ_q between 10 and 50 ms. Red-dashed line is the fitting for τ_q between 150 and 1000 ms. A power law $N_q = \tau_q^{-\alpha}$ fits for the data points of the black-solid line gives $\alpha = 0.25 \pm 0.05$. The same law for the data points of the red-dashed line gives $\alpha = 0.42 \pm 0.04$. Inset: Domains number N_q for quench time 1 ms $< \tau_q <$ 100 ms. The shaded area indicates HKZM is invalid.

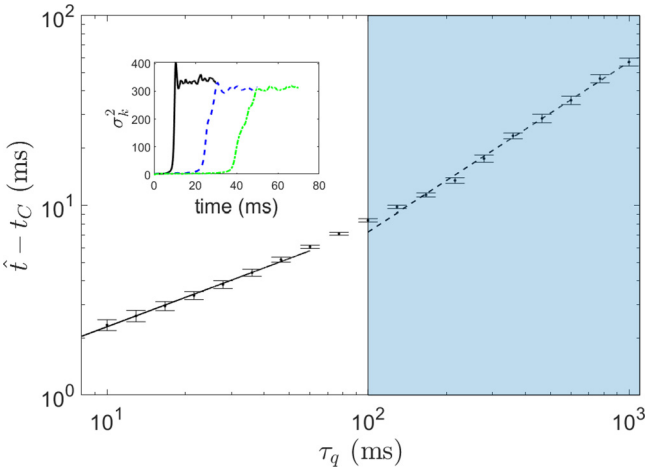

FIG. 4. $\hat{t} - t_C$ versus quench time τ_q, these data are extracted from the second moment of momentum distribution. Black solid line is the fitting curve $\ln(\hat{t} - t_C) \sim -\frac{\nu z}{1+\nu z} \ln \tau_q$, the fitting parameter is $\frac{\nu z}{1+\nu z} = 0.52 \pm 0.03$ for quench time τ_q between 10 and 50 ms, and $\frac{\nu z}{1+\nu z} = 0.89 \pm 0.05$ for quench time τ_q between 150 and 1000 ms. Inset: Second moment of momentum distribution σ_k^2 versus time for quench time $\tau_q = 10$ ms (black solid line), $\tau_q = 30$ ms (blue dashed line), and $\tau_q = 50$ ms (green dash-dotted line). The shaded area indicates HKZM is invalid.

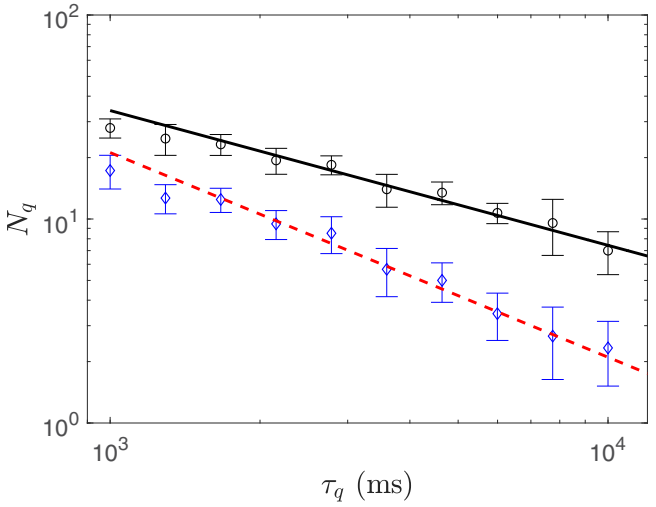

FIG. 5. Domains number N_q versus quench time τ_q. Circles and diamonds with error bar correspond to numerical results for region $R = R_{\rm TF}$ and for region $R = 0.6R_{\rm TF}$, respectively. Black-solid and red-dashed lines are the fittings. A power law $N_q = \tau_q^{-\alpha}$ fitting for the data points of the black-solid line gives $\alpha = 0.66 \pm 0.14$, the same law for the data points of the red-dashed line gives $\alpha = 1.00 \pm 0.16$.

the domains number and frozen time will not follow the prediction of HKZM, as seen in Figs. 3 and 4.

To gain a better understanding of the effect of the trap and the IKZM, we simulated the quench process for longer quench times, and we quench Ω without position-dependent to maximally exploit the inhomogeneity of the system. In Fig. 5, we plotted the numerical results for simulation with quench times ranging from 10^3 to 10^4 ms. In this case, the HKZM always give the wrong scaling exponents. The trapping potential gives a smaller Thomas-Fermi radius, which reduces the speed of front [Eq. (12)], and according to [33], the scaling exponent should obey $N_q \sim \tau_q^{-\frac{1+2\nu}{1+z\nu}}$ provided the density profile can be calculated via Thomas-Fermi approximation, but this N_q should only take into account a very small region and this region's radius depends on the quench times. In Fig. 5, the black circles was obtained by taking account of all the defects inside the Thomas-Fermi radius, the fitting gives us a scaling exponent $\alpha = 0.66 \pm 0.14$. The red-dashed line is the fitting for the data obtained within $R = 0.6R_{\rm TF}$, the fitting gives us a scaling exponent $\alpha = 1.0 \pm 0.16$, which is consistent with prediction of IKZM, where $\nu = \frac{1}{2}$ and $z = 2$ for our system. The scaling exponent obtained here conforms that we need to only consider a small region instead. Our findings suggest that the HKZM only works for weak-enough trap potential and fast-enough quench times [32,41,42].

V. DISCUSSION

We studied HKZM and IKZM in a trapped BEC with SOC within the framework of truncated-Winger GPE and observed domains formation in the quench process, we extracted two power laws from the formation time and domains number data. We get two scaling exponents ν and z. In our scheme, the defects are formed in spatial space which makes it easier to detect in experiments. The SOC effect can be viewed as follows. The Rabi coupling term acts like a magnetic field pointing in the x axis

$$B \sim \begin{pmatrix} 0 & \Omega \\ \Omega & 0 \end{pmatrix}. \tag{31}$$

As we linearly decrease Ω, the system will feel a equivalent vortex electric field around the x axis, the particles will rotate around x axis. There will be no shear flows since the whole system is superfluity. This scenario changes after Ω crosses the critical point, the superfluid density decays to zero as Ω approaches the critical point. The shear flows will form since the viscosity eventually restores. The smaller the quench time τ_q is, the larger the vortex electric field is, and the width of the shear flow decreases as the τ_q decreases. In our case, widths of the shear flows are just the defects sizes.

Compared to the study of KZM in the Landau-Zener system [3] or in the Ising model [6], our system includes the interaction which makes it a many-body system instead of single-particle system. Also, to make the system more experimentally realistic, we included a harmonic trap potential.

In the experiment found in [43,44], they used two hyperfine states $|1\rangle = |F = 1, m_F = +1\rangle$ and $|2\rangle = |F = 1, m_F = -1\rangle$ of ^{87}Rb as the two pseudospin states. These two hyperfine states have a property $g_{11} \approx g_{22}$ and they can tune g_{12} to be very close to g_{11}. For $N = 10^4$, $\omega_x = 2\pi \times 5$ Hz, $\omega_y = \omega_z = 2\pi \times 2$ kHz [40], the Thomas-Fermi radius is $R_{\rm TF} \approx 115\ \mu$m, the healing length at the trap center is about $\xi = \sqrt{\frac{\hbar^2}{2mn(0)g}} \approx 0.2\ \mu$m, the spin healing length $\xi_s = \sqrt{\frac{\hbar^2}{2mn(0)|g_s|}}$ is about 4.5ξ, there are about $N_d^{\rm max} \sim 250$ defects maximum in our system. So our scheme is feasible to be realized in the experiment with current technology.

ACKNOWLEDGMENTS

The authors acknowledge very valuable help by Blair Blakie on numerical methods and the manuscript, we also thank Xiangfa Zhou and Chuanwei Zhang for valuable discussions. This work is supported by National Key R&D Program (No. 2016YFA0301300 and No. 2016YFA0501700), National Natural Science Foundation of China (No. 11674306 and No. 61590932), and Anhui Initiative in Quantum Information Technologies.

[1] T. W. B. Kibble, J. Phys. A: Math. Gen. **9**, 1387 (1976).
[2] W. H. Zurek, Nature **317**, 505 (1985).
[3] B. Damski, Phys. Rev. Lett. **95**, 035701 (2005).
[4] B. Damski and W. H. Zurek, Phys. Rev. A **73**, 063405 (2006).
[5] B. Damski and W. H. Zurek, Phys. Rev. Lett. **104**, 160404 (2010).
[6] J. Dziarmaga, Phys. Rev. Lett. **95**, 245701 (2005).
[7] C. Lee, W. Hai, L. Shi, and K. Gao, Phys. Rev. A **69**, 033611 (2004).

[8] J. Xu, S. Wu, X. Qin, J. Huang, Y. Ke, H. Zhong, and C. Lee, Europhys. Lett. **113**, 50003 (2016).
[9] C. Lee, Phys. Rev. Lett. **102**, 070401 (2009).
[10] A. Lamacraft, Phys. Rev. Lett. **98**, 160404 (2007).
[11] H. Saito, Y. Kawaguchi, and M. Ueda, Phys. Rev. A **76**, 043613 (2007).
[12] S. Wu, Y. Ke, J. Huang, and C. Lee, Phys. Rev. A **95**, 063606 (2017).
[13] M. Anquez, B. A. Robbins, H. M. Bharath, M. Boguslawski, T. M. Hoang, and M. S. Chapman, Phys. Rev. Lett. **116**, 155301 (2016).
[14] M. Uhlmann, R. Schützhold, and U. R. Fischer, Phys. Rev. Lett. **99**, 120407 (2007).
[15] Q. Ye, S. Wu, X. Jiang, and C. Lee, J. Stat. Mech.: Theory Exp. (2018) 053110.
[16] I. Chuang, R. Durrer, N. Turok, and B. Yurke, Science **251**, 1336 (1991).
[17] C. N. Weiler, T. W. Neely, D. R. Scherer, A. S. Bradley, M. J. Davis, and B. P. Anderson, Nature **455**, 948 (2008).
[18] L. W. Clark, L. Feng, and C. Chin, Science **354**, 606 (2016).
[19] G. Labeyrie and R. Kaiser, Phys. Rev. Lett. **117**, 275701 (2016).
[20] X.-Y. Xu, Y.-J. Han, K. Sun, J.-S. Xu, J.-S. Tang, C.-F. Li, and G.-C. Guo, Phys. Rev. Lett. **112**, 035701 (2014).
[21] K. Pyka, J. Keller, H. L. Partner, R. Nigmatullin, T. Burgermeister, D. M. Meier, A. Retzker, M. B. Plenio, W. H. Zurek, A. del Campo, and T. E. Mehlstäubler, Nat. Commun. **4**, 2291 (2013).
[22] K. Baumann, R. Mottl, F. Brennecke, and T. Esslinger, Phys. Rev. Lett. **107**, 140402 (2011).
[23] S. C. Chae, N. Lee, Y. Horibe, M. Tanimura, S. Mori, B. Gao, S. Carr, and S.-W. Cheong, Phys. Rev. Lett. **108**, 167603 (2012).
[24] C. V. Parker, L.-C. Ha, and C. Chin, Nat. Phys. **9**, 769 (2013).
[25] D. L. Campbell, R. M. Price, A. Putra, A. Valdés-Curiel, D. Trypogeorgos, and I. B. Spielman, Nat. Commun. **7**, 10897 (2016).
[26] Y. J. Lin, K. Jimenez-Garcia, and I. B. Spielman, Nature **471**, 83 (2011).
[27] T.-L. Ho and S. Zhang, Phys. Rev. Lett. **107**, 150403 (2011).
[28] Y. Li, L. P. Pitaevskii, and S. Stringari, Phys. Rev. Lett. **108**, 225301 (2012).
[29] Y. Li, G. I. Martone, L. P. Pitaevskii, and S. Stringari, Phys. Rev. Lett. **110**, 235302 (2013).
[30] C. Hamner, C. Qu, Y. Zhang, J. Chang, M. Gong, C. Zhang, and P. Engels, Nat. Commun. **5**, 4023 (2014).
[31] W. H. Zurek, Phys. Rev. Lett. **102**, 105702 (2009).
[32] F. J. Gomez-Ruiz and A. del Campo, Phys. Rev. Lett. **122**, 080604 (2019).
[33] A. del Campo, T. W. B. Kibble, and W. H. Zurek, J. Phys.: Condens. Matter **25**, 404210 (2013).
[34] B. Damski and W. H. Zurek, Phys. Rev. Lett. **99**, 130402 (2007).
[35] P. B. Blakie, A. S. Bradle, M. J. Davis, R. J. Ballagh, and C. W. Gardiner, Adv. Phys. **57**, 363 (2008).
[36] P. G. de Gennes, *Superconductivity of Metals and Alloys* (Cambridge University Press, Cambridge, England, 1999).
[37] L. Pitaevskii and S. Stringari, *Bose-Einstein Condensation and Superfluidity*, 2nd ed. (Oxford University Press, London, 2016).
[38] C. Gardiner and P. Zoller, *Quantum Noise: A Handbook of Markovian and Non-Markovian Quantum Stochastic Methods with Applications to Quantum Optics*, 3rd ed. (Springer-Verlag, Berlin, 2004).
[39] G. de Chiara, A. del Campo, G. Morigi, M. B. Plenio, and A. Retzker, New J. Phys. **12**, 115003 (2010).
[40] J. Sabbatini, W. H. Zurek, and M. J. Davis, Phys. Rev. Lett. **107**, 230402 (2011).
[41] H. Saito, Y. Kawaguchi, and M. Ueda, J. Phys.: Condens. Matter **25**, 404212 (2013).
[42] A. del Campo, A. Retzker, and M. B. Plenio, New J. Phys. **13**, 083022 (2011).
[43] M. Erhard, H. Schmaljohann, J. Kronjäger, K. Bongs, and K. Sengstock, Phys. Rev. A **69**, 032705 (2004).
[44] S. Tojo, Y. Taguchi, Y. Masuyama, T. Hayashi, H. Saito, and T. Hirano, Phys. Rev. A **82**, 033609 (2010).